49th AIAA Aerospace Sciences Meeting including the New Horizons Forum and Aerospace Exposition
4 - 7 January 2011, Orlando, Florida

AIAA 2011-1248

Adjoint based aerodynamic optimization of supersonic biplane airfoils

Rui Hu*
Massachusetts Institute of Technology, Cambridge, MA 02139, USA

Antony Jameson†
Stanford University, Stanford, CA 94305, USA,

Qiqi Wang‡
Massachusetts Institute of Technology, Cambridge, MA 02139, USA

This paper addresses the aerodynamic performance of Busemann type supersonic biplane at off-design conditions. An adjoint based optimization technique is used to optimize the aerodynamic shape of the biplane to reduce the wave drag at a series of Mach numbers ranging from 1.1 to 1.7, at both acceleration and deceleration conditions. The optimized biplane airfoils dramatically reduces the effects of the choked flow and flow-hysteresis phenomena, while maintaining a certain degree of favorable shockwave interaction effects at the design Mach number. Compared to a diamond shaped single airfoil of the same total thickness, the wave drag of our optimized biplane is lower at almost all Mach numbers, and is significantly lower at the design Mach number.

I. Introduction

For decades, the speed of commercial aircraft was constrained by the sound barrier. Even with the most successful Concorde, supersonic flight was only available on a small number routes and for those are willing and able to pay for the expensive airplane tickets. The two major challenges for supersonic flight are high drag due to shock waves and the sonic boom.

The biplane concept proposed by Adolf Busemann[1] can potentially solve both the high drag and the sonic boom problems. At the design condition, the Busemann biplane produces zero wave drag and no sonic boom will escape from the biplane system due to the wave cancellation between two airfoil components. Much research was performed on the Busemann biplane concept from 1935 to 1960's. Moeckel[2] and Licher[3] developed optimized lifting supersonic biplanes by theoretical analysis. Furthermore, Tan[4] calculated analytical expressions for the drag and lift of a three dimensional supersonic biplane with finite span and rectangular planer shape. Ferri[5] obtained some experimental results of the aerodynamic characteristics of the supersonic biplane using the wind tunnel and compared them with the analytical results. Currently there is renewed interest in supersonic biplane airfoils. Igra and Arad[6] tested different parameters' effect on the drag coefficient of the Busemann airfoil at various flow conditions. Recently, Kusunose proposed using the Busemann's biplane concept to the next generation supersonic transport design. His research group carried out a series of studies including both computational fluid dynamic (CFD) methods and wind tunnel experimental methods.[7–12]

*Corresponding author, Postdoctoral Associate, Aeronautics and Astronautics, Cambridge, MA, USA
†Professor, Aeronautics and Astronautics, Stanford, CA, USA, AIAA member
‡Assistant Professor, Aeronautics and Astronautics, Cambridge, MA, USA, AIAA member

Although the Busemann airfoil demonstrates very good performance at the design Mach number, the drag of the Busemann airfoil at the off-design conditions is much higher due to the choked-flow phenomenon. An even worse problem for the off-design Busemann airfoil is the flow-hysteresis phenomenon. In order to alleviate these problems of the Busemann airfoil, Kusunose et al[10] proposed a configuration with leading and trailing edge flaps.

In this paper, we use multiple point adjoint based aerodynamic design and optimization method to improve the baseline Busemann biplane airfoil's off-design performance and alleviate the flow hysteresis problem. The adjoint method efficiently solves the every high dimensional design problem and thus can find the true optimal aerodynamic shape that maintenance superior design point performance and significantly improve the off-design performance.

II. Busemann Type Biplane – Design Point Performance

A. The Wave drag of Supersonic Thin Airfoil

Based on the physical origins of the drag components, the total drag of a wing can be divided into several components: skin friction drag, wave drag, pressure drag and vortex drag. In supersonic cruise flight, the wave drag, the drag due to the presence of shock waves, is dominant.

The shock-expansion theory can be used to solve the lift and drag of an airfoil in supersonic flow. If the airfoil is thin and the angle of attack is small, then the lift and drag can be approximately given as simple analytical expressions via the thin airfoil theory.[13] We define the lift and drag coefficients as

$$c_l = \frac{L}{qc}, \quad c_d = \frac{D}{qc}$$

where L and D are the lift and wave drag of the air foil respectively. And q represents the dynamic pressure, which is

$$q = \frac{1}{2}\rho_\infty U_\infty^2$$

Then according to thin airfoil theory, c_l and c_d for an arbitrary two-dimensional airfoil (as shown in Figure 1) can be given as:

$$\begin{aligned} c_l &= \frac{4\alpha_0}{\sqrt{M_\infty^2 - 1}} \\ c_d &= \frac{4}{\sqrt{M_\infty^2 - 1}} \left[\overline{(\frac{dh}{dx})^2} + \alpha_0^2 + \overline{\alpha_c^2(x)} \right] \end{aligned} \tag{1}$$

From the above equation, it is clear that the lift of this general thin airfoil in supersonic flow only depends on the mean angle of attack. And the wave drag of this airfoil can be split into three parts: drag caused by angle of attack, drag caused by camber and drag caused by thickness. The wave drag in the 2-D case can only be reduced separately according to the different generation mechanism.[13]

B. Busemann Airfoil

Adolf Busemann[1] proposed a biplane concept by simply dividing a diamond airfoil into two components and placing the triangular surfaces facing each other (Figure 2). The Busemann airfoil is an excellent design to reduce the drag due to life (refer as wave reduction effect) and also the drag due to thickness (refer as wave cancellation effect).

1. Wave Reduction Effect

The drag due to lift (including the drag caused by angle of attack and the drag caused by airfoil camber) can not be eliminated completely. But this part of the drag can be reduced significantly by combining multiple

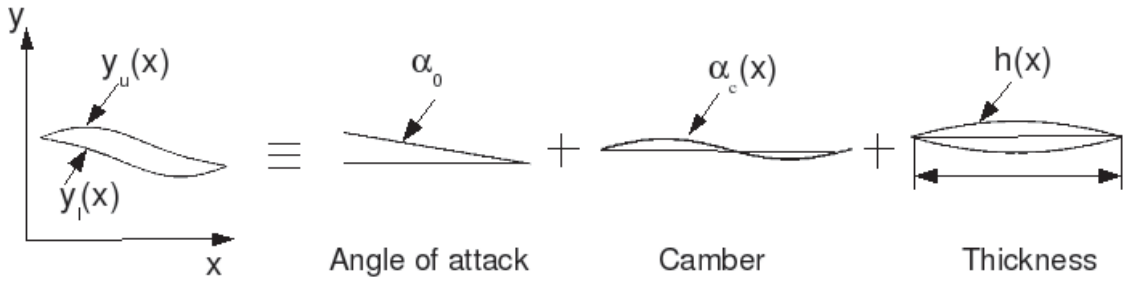

Figure 1. Linear resolution of arbitrary airfoil into lift, camber, and drag[13]

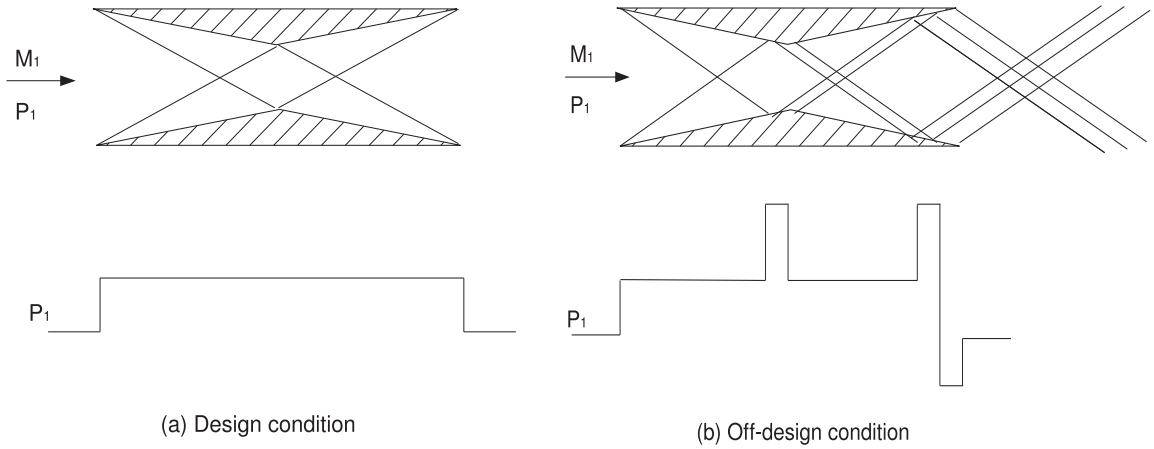

Figure 2. Design vs off-design condition of the Busemann biplane

airfoils together.[7] To show this, we first simplify the general airfoil to a flat plate airfoil. Thus c_l is the same as given in equation (1) and c_d is reduced to

$$c_d = \frac{4\alpha_0^2}{\sqrt{M_\infty^2 - 1}} \tag{2}$$

We can see clearly that for a flat plate, the lift coefficient is proportional to the angle of attack while the drag coefficient is proportional to the square of the angle of attack.

Considering an airfoil consists of n parallel flat plates with the same chord length c as the single flat plate airfoil, as shown in Figure 3. To set the total lift of this n-plates airfoil equal the lift of the single plate airfoil, the angle of attack α_n should be $\alpha_n = \alpha_0/n$. Thus,

$$c_{ln} = n \cdot \frac{4\alpha_n}{\sqrt{M_\infty^2 - 1}} = n \cdot \frac{4\alpha_0/n}{\sqrt{M_\infty^2 - 1}} = c_{ls}.$$

Similarly, the wave drag of this n-plates airfoil equal the summation of the wave drag of each individual plate

$$c_{dn} = n \cdot \frac{4\alpha_n^2}{\sqrt{M_\infty^2 - 1}} = n \cdot \frac{4(\alpha_0/n)^2}{\sqrt{M_\infty^2 - 1}} = \frac{1}{n}\frac{4\alpha_0^2}{\sqrt{M_\infty^2 - 1}} = \frac{1}{n}c_{ds}$$

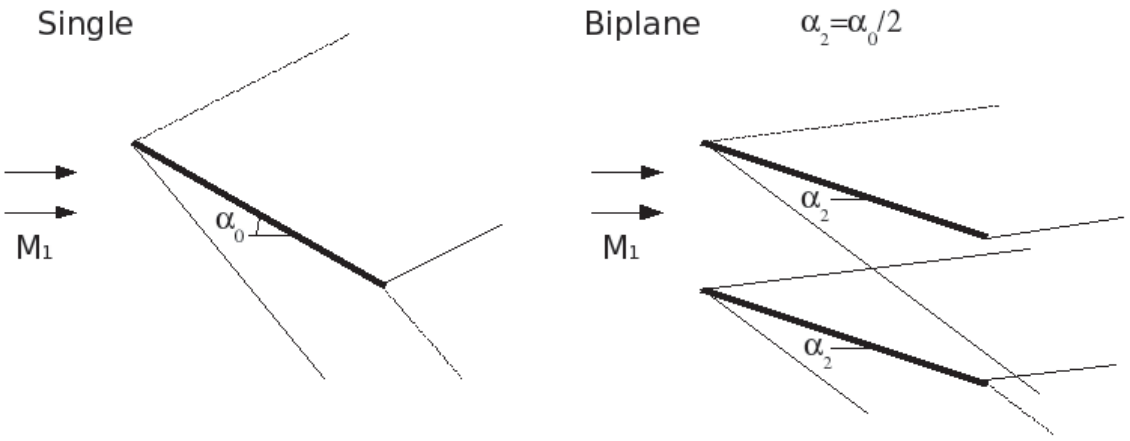

Figure 3. Wave reduction effect

From the above equation, we can see that the wave drag of the n-plate airfoil is only $\frac{1}{n}$ of that of a single plate airfoil with the same lift. However, we also should notice that the increased surface area of the multiple airfoil combination will produce more skin-friction drag.

For a multiple airfoil combination configuration, the lift of the individual airfoil will be reduced so that the drag caused by lift will be reduced, while the total lift of the multiple airfoil will not be reduced but only be re-distributed. This is called as the "wave reduction effect" by Kusunose et al in their paper.[7]

2. Wave Cancellation Effect

The drag due to thickness can also be significantly reduced by introducing the biplane configuration. By adjusting the distance between the two airfoils at a given Mach number, the strong shock wave generated at the leading edge will exactly reach the inner corner point of the opposite airfoil and will be canceled by the expansion wave at that point. At the design condition, theoretically the shock waves can be completely canceled so that zero wave drag is produced, as shown in Figure 4.

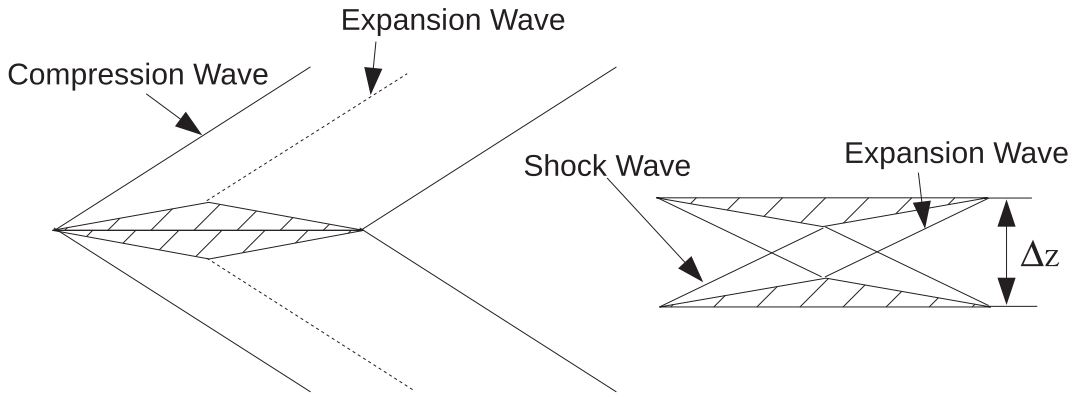

Figure 4. Wave cancellation effect

However, at design point, because of the entropy increase caused by the shock wave inside the biplane system (as shown in Figure 4) and the non-linear effect during the shock-expansion wave interaction processes,[13,14] the zero wave drag condition of the Busemann airfoil design will not be actually realized. Kusunose[15] introduces the Oswatitsch's wave drag expression which can be used to predict this internal shock wave related wave drag. This part of the drag can be given as

$$D_w = P_\infty \int \frac{\Delta s}{R} dz = P_\infty \int \left(-ln \frac{P_0}{P_{0\infty}} \right) dz$$

where, Δs and $\frac{P_0}{P_{0\infty}}$ denote entropy production and the total pressure deficit through shock waves.

At other Mach numbers, the shock wave will only be partially canceled, as shown in Figure 2. Therefore, the wave drag will not be zero anymore in the off design case. We will discuss the off design conditions in more detail in next section.

3. Wave Reflection Effect

There is another attractive property of biplane airfoil design. The configuration can be arranged so that the shock wave is reflected to the sky and does not reach the ground, and consequently the sonic boom will be dramatically reduced as shown in Figure 5.

However, according to thin airfoil theory, the lift of the biplane system is reduced due to this shock wave reflection. Using CFD Kusunose et al proved in their paper,[7] the lift of the biplane system will be zero if all the shock waves are reflected into the sky. Airfoils producing zero lift are not practically useful. Also, because of the poor lift to drag ratio (L/D), as shown in Figure 6, the simple shock reflection biplane will not satisfy the low drag and low boom requirements for the supersonic flight.

Liepmann[13] examines several different biplane examples to optimize the ratio D/L^2. Because at a lifting condition, there is a wave drag due to lift, the wave drag of the Busemann biplane is no longer zero. To obtain a beneficial shock-expansion wave interaction, the lift, thickness and camber effects must be considered together.

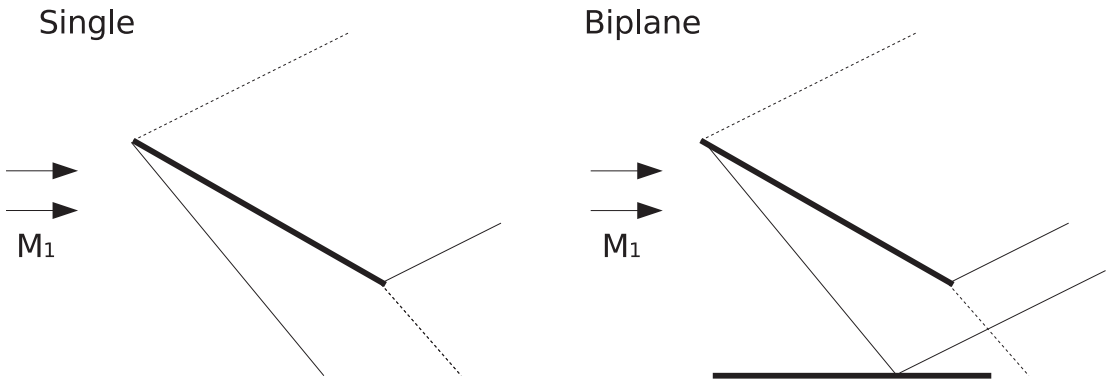

Figure 5. Wave reflection effect

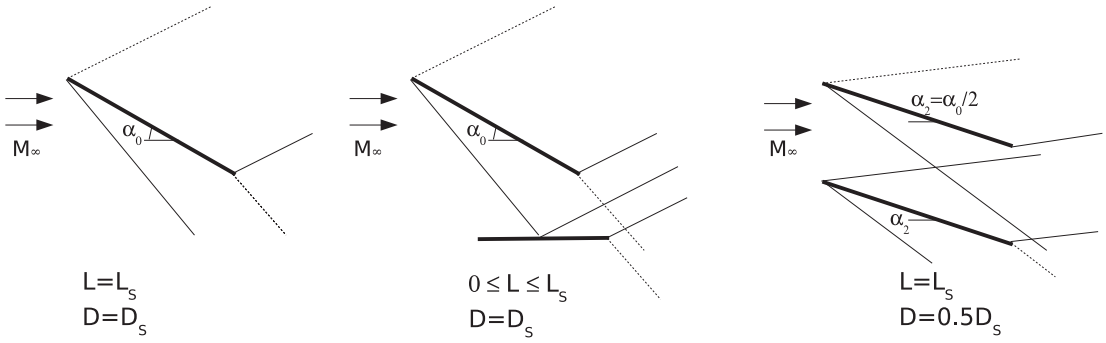

Figure 6. L/D ratio reduction due to the wave reflection effect

III. Off-Design Condition of the Busemann Airfoil

As discussed above, the Busemann biplane airfoil produces very small wave drag at the design condition. However, at off-design conditions, the Busemann airfoil shows very poor aerodynamic performance. Here, we use computational fluid dynamics (CFD) method to demonstrate this. The configurations of the baseline diamond airfoil and the Busemann biplane airfoil are given in Figure 7.

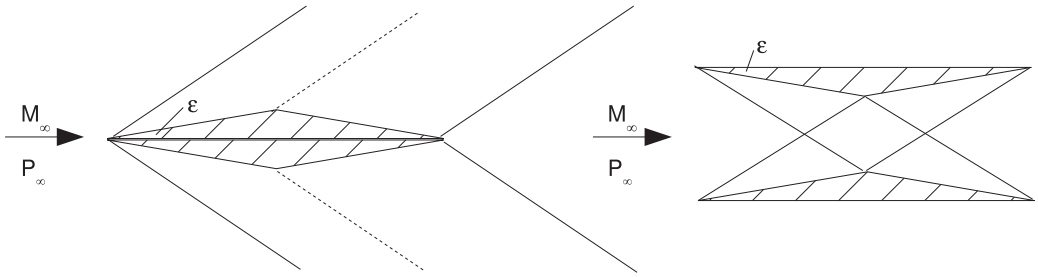

(a) The baseline diamond airfoil (b) The Busemann biplane airfoil

Figure 7. Configuration comparison

Figure 8 shows the comparison of the drag coefficient(c_d) for these two airfoils over a range of Mach numbers. In these calculations, an impulsive start from uniform flow is used as the initial condition.

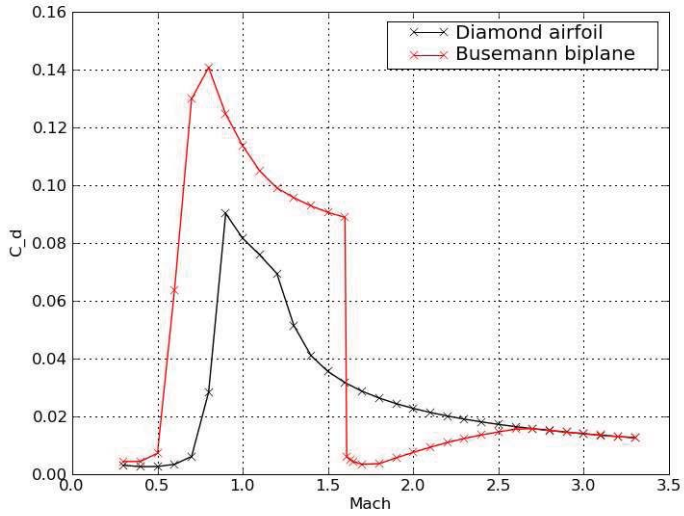

Figure 8. c_d plot for different airfoils at zero-lift condition.

As can be seen, when the Mach number is small (lower than 1.6 in the plot), the drag for the Busemann airfoil is higher than that of the diamond airfoil. But in the range of Mach numbers from 1.61 to 2.7, the drag coefficient for the Busemann airfoil becomes lower than that of the diamond airfoil. Especially at Mach

number 1.7, which is the design condition for this Busemann airfoil, $c_d = 0.00341$. Due to the favorable shock-shock interaction effect, it is possible for the Busemann airfoil to produce much smaller drag (the red line in the plot) near the design Mach number than the standard diamond airfoil does. This is the advantage of using the Busemann airfoil design.

These calculations verify that the Busemann airfoil demonstrates very good performance at the design Mach number. But for the off-design conditions, the drag of the Busemann airfoil can be much higher because of the choked-flow phenomenon. Figure 9 shows the pressure field around the Busemann airfoil under two different off-design Mach numbers. In the case of $M_\infty < 1.0$, as given in Figure 9 (a), the flow becomes sonic at the mid-chord apex and is further accelerated to supersonic. Then a vertical shock wave is formed at the trailing edge of the biplane airfoil. The high wave drag of this Mach number condition is due to the low pressure of the rear part of the airfoil. In the case of $1.0 < M_\infty < 1.6$, as given in Figure 9 (a), the flow condition is different. A strong bow shock wave is formed in front of the leading edge and the flow is choked. The flow behind the bow shock wave becomes subsonic and a high pressure field is built so that the wave drag of this off-design condition is also very high.

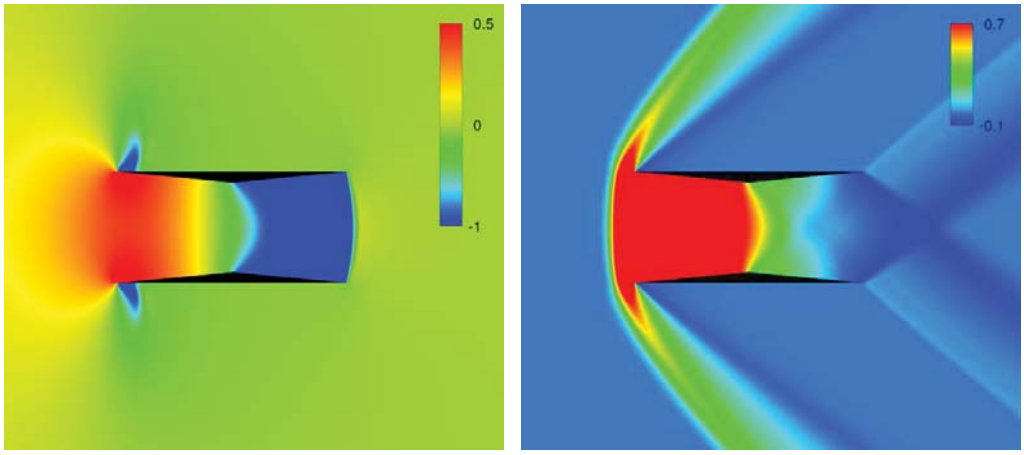

(a) M_∞ =0.8 (b) $M_\infty = 1.6$

Figure 9. Pressure field of the Busemann airfoil under off-design Mach numbers

However, there are even worse problem for the off-design conditions of the Busemann airfoil due to the flow-hysteresis phenomenon. If we slowly accelerate the flow by using the previous simulation result as the initial condition, we obtain a new c_d plot versus Mach number as Figure 10. From the plot we can see two separated c_d lines in the range near Mach number 1.6 to Mach number 2.1 for the Busemann airfoil. The green line shows the c_d of the Busemann airfoil during acceleration and the red one shows the c_d during deceleration, which are due to the flow-hysteresis phenomenon during acceleration and the choked-flow phenomenon during deceleration.

IV. Numerical Methods for Optimizing Off-Design Condition

The Euler equations for compressible inviscid flows can be written in an integral form

$$\frac{\partial}{\partial t}\iint_S w dS + \int_{\partial S}(f dy - g dx) = 0 \tag{3}$$

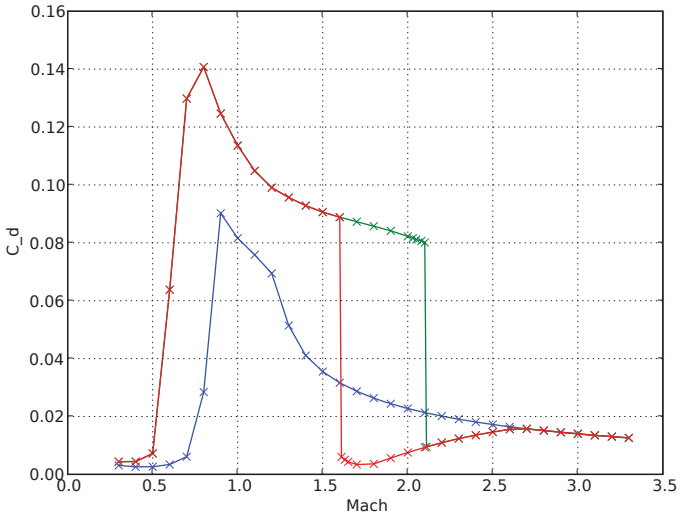

Figure 10. c_d **plot for different airfoils at zero-lift condition.**

for a domain S with boundary ∂S, where w represents the conserved quantities, and f and g represent the fluxes in x and y directions respectively:

$$w = \begin{pmatrix} \rho \\ \rho u \\ \rho v \\ \rho E \end{pmatrix}, \quad f = \begin{pmatrix} \rho u \\ \rho u^2 + p \\ \rho uv \\ \rho uH \end{pmatrix}, \quad g = \begin{pmatrix} \rho v \\ \rho vu \\ \rho v^2 + p \\ \rho vH \end{pmatrix}. \tag{4}$$

In this paper, we use second order finite volume space discretization. A blended first and third order flux artificial dissipation proposed by Jameson, Schmidt and Turkel[16] is applied. The coefficients of these differences depend on the local pressure gradient. Since we don't care about the details of the transient solution, and the only objective here is to reach a steady state as fast as possible, the time integration schemes with a fast convergence property are chosen. In this research, we use a modified Runge-Kutta approach introduced by Jameson.[17] This scheme has been successfully applied to both structured and unstructured mesh problems.[16,18,19] To further accelerate the convergence, the multigrid scheme is used, which is developed by Jameson to efficiently solve hyperbolic equations.[18,20]

For this off-design conditions design problem, the geometry of the airfoil is defined by a set of shape parameters. The cost function, which is also a function of the shape parameters, is chosen as the drag coefficient or the lift to drag ratio. The gradient is needed to determine a direction of improvement. The disadvantage of using finite difference scheme to find the gradient is the huge computational cost because for each design variable the flow is recalculated to estimate the gradient. Using control theory the gradient can be determined by solving a single adjoint equation, the cost of which is comparable to that of solving the flow equation.

Assume the cost function I

$$I = I(w, \mathcal{F}) \tag{5}$$

The change of the cost function due to a change in $\mathcal{F}$ is:

$$\delta I = \left[\frac{\partial I^T}{\partial w}\right]_I \delta w + \left[\frac{\partial I^T}{\partial \mathcal{F}}\right]_{II} \delta \mathcal{F} \tag{6}$$

Here, the subscripts I represents the change related to the variation δw in the flow field and II represents the change caused by the shape modification $\delta\mathcal{F}$.

The governing equation R can also be written as function of w and $\mathcal{F}$ within the flow field domain D:

$$R(w, \mathcal{F}) = 0 \tag{7}$$

Then δw is determined from the equation

$$\delta R = \left[\frac{\partial R}{\partial w}\right]_I \delta w + \left[\frac{\partial R}{\partial \mathcal{F}}\right]_{II} \delta\mathcal{F} = 0 \tag{8}$$

Because the variation δR equals zero, it can be multiplied by a Lagrange Multiplier ψ and subtracted from the variation δI without changing the result. Thus, equation (6) can be rewritten as

$$\begin{aligned}\delta I &= \frac{\partial I^T}{\partial w}\delta w + \frac{\partial I^T}{\partial \mathcal{F}}\delta\mathcal{F} - \psi^T\left(\left[\frac{\partial R}{\partial w}\right]\delta w + \left[\frac{\partial R}{\partial \mathcal{F}}\right]\delta\mathcal{F}\right) \\ &= \left\{\frac{\partial I^T}{\partial w} - \psi^T\left[\frac{\partial R}{\partial w}\right]\right\}_I \delta w + \left\{\frac{\partial I^T}{\partial \mathcal{F}} - \psi^T\left[\frac{\partial R}{\partial \mathcal{F}}\right]\right\}_{II} \delta\mathcal{F}.\end{aligned} \tag{9}$$

where ψ is chosen to satisfy the adjoint equation

$$\left[\frac{\partial R}{\partial w}^T\right]\psi = \frac{\partial I}{\partial w}$$

Now the first term in equation (9) is eliminated and δI can be given as

$$\delta I = \mathcal{G}\delta\mathcal{F} \tag{10}$$

where

$$\mathcal{G} = \frac{\partial I^T}{\partial \mathcal{F}} - \psi^T\left[\frac{\partial R}{\partial \mathcal{F}}\right]$$

Since equation (10) is independent of δw, the gradient of I with respect to an arbitrary number of design variables can be determined without the need to resolve the flow equation. Once the gradient vector $\mathcal{G}$ has been obtained, it may be used to determine the direction of improvement.

Since the gradient $\mathcal{F}$ from above equation is generally less smooth than the shape, we use smoothed sobolev gradient instead to optimize the problem.

For example, if we want to apply smoothing in the ξ_1 direction, the smoothed gradient $\bar{\mathcal{G}}$ can be calculated from a discrete approximation to

$$\bar{\mathcal{G}} - \frac{\partial}{\partial\xi_1}\epsilon\frac{\partial}{\partial\xi_1}\bar{\mathcal{G}} = \mathcal{G},$$

where ϵ is the smoothing parameter. Then we replace $\mathcal{G}$ by its smoothed value $\bar{\mathcal{G}}$ and set

$$\delta\mathcal{F} = -\lambda\bar{\mathcal{G}}.$$

Then we assume the modification is applied on the surface $\xi_2 =$ constant, the first order change in the cost function is

$$\begin{aligned}\delta I &= -\iint \mathcal{G}\delta\mathcal{F}d\xi_1 d\xi_3 \\ &= -\lambda\iint\left(\bar{\mathcal{G}} - \frac{\partial}{\partial\xi_1}\epsilon\frac{\partial\bar{\mathcal{G}}}{\partial\xi_1}\right)\bar{\mathcal{G}}d\xi_1 d\xi_3 \\ &= -\lambda\iint\left(\bar{\mathcal{G}}^2 + \epsilon\left(\frac{\partial\bar{\mathcal{G}}}{\partial\xi_1}\right)^2\right)d\xi_1 d\xi_3 \\ &< 0.\end{aligned}$$

If λ is a sufficiently small positive, above equation will guarantee an improvement until the decent process reach a stationary point at which $\mathcal{G} = 0$. Conventional optimization methods assume that the design variables are completely independent. However, for our optimization case, the mesh points are used as the design variables, which can not be moved independently due to the shape smoothness requirement. Thus, gradient smoothing is important and necessary. Also, the above optimization algorithm is based entirely on driving the gradient to zero and does not directly measure the cost function. It is possible the gradient could reach zero at a local minimum. For the two dimensional inviscid transonic airfoil optimization problem, however, the drag is almost invariably reduced to zero corresponding to a shock free shape. But the final optimized shape is not unique and depends on the initial shape.

V. Supersonic Biplane Airfoil Optimization Results

The results of the optimized Busemann type biplane airfoil at both zero-lifting and lifting conditions are showed. To test the sensitivity, two cases are studied and we found that the optimized design is robust and not very sensitive to changes in the angle of attack or the separation distance.

A. Original Busemann Airfoil Design

Firstly, the standard diamond airfoil and the Busemann airfoil are calculated at the zero-lift condition. To make the results comparable, the total airfoil thickness of these two airfoils are set the same value. Here, the thickness-chord ratio of the diamond airfoil is t/c=0.1, while the thickness-chord ratio of the the Busemann airfoil are t/c=0.05 for each component. The distance between two Busemann airfoils is set to half of the chord length in order to obtain the theoretical minimum drag for the designed Mach number 1.7. The angle of attack of both airfoils are set to zero.

Figure 11 shows the H mesh of the Busemann airfoils used for calculation. The grid numbers before the airfoil and after the airfoil in the horizontal direction are both 64. In the vertical direction, the grid between the two components is 64×64.

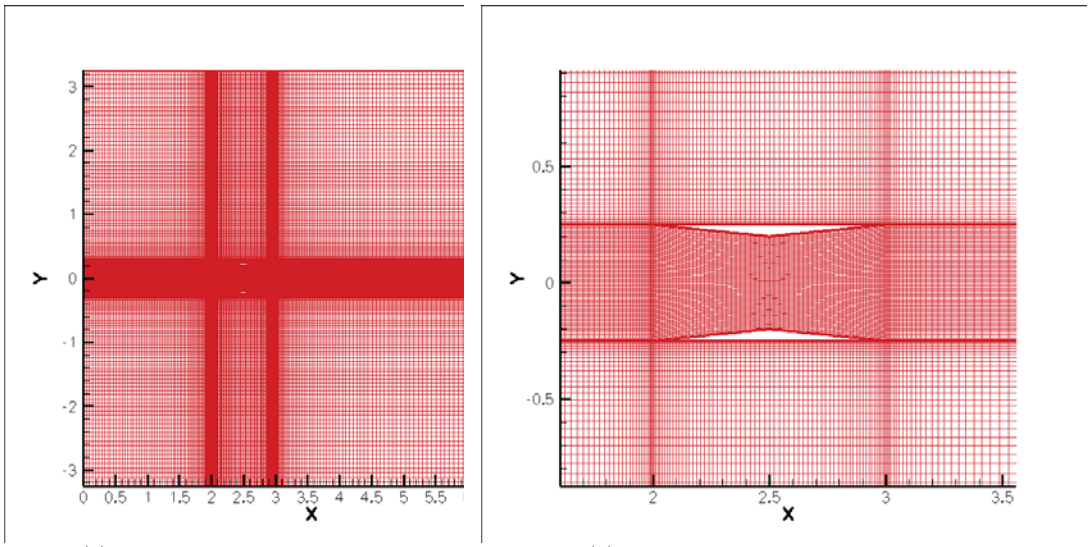

(a) Mesh for Busemann airfoil (b) Mesh for Busemann airfoil zoom in

Figure 11. Grid configuration for calculation

The analytical results obtained by the supersonic thin airfoil theory are given in Table 1 and the numerical results calculated by current method are given in Table 2. Comparing these two tables, we can see that the numerical results are generally in good agreement with the analytical results. Because of the wave

cancellation effect, the wave drag of the Busemann airfoil is much lower than those of other two airfoils. However, we also find that the wave drag of the Busemann airfoil can not be completely eliminated due to the non-linear effect as we discussed before.

	c_l	c_d
Diamond airfoil	0.0000	0.0291
Busemann biplane airfoil	0.0000	0.0000

Table 1. Theoretical lift and drag coefficients of different airfoils

	c_l	c_d
Diamond airfoil	0.0000	0.0287
Busemann biplane airfoil	0.0000	0.0034

Table 2. Numerical lift and drag coefficients of different airfoils

Next we examine at the detailed conditions for the flow-hysteresis phenomenon during acceleration and the choked-flow phenomenon during deceleration of the Busemann airfoil. Figure 12 shows the pressure coefficient of the Busemann airfoil during acceleration. The angle of attack is set to zero and the resulting non-lifting flow field is shown at various supersonic Mach numbers. As can be seen, at Mach numbers up to 2.1, there is a bow shock wave in front of the airfoil. After the bow shock wave, there is a subsonic region between the two airfoils where the pressure coefficient is high (marked by red). This bow shock results in substantially (an order of magnitude) higher drag than at the design condition. When the Mach number increases from 2.1 to 2.11, the bow shock wave is swallowed into the two airfoils and replaced by two oblique shock waves, and the subsonic region between the two airfoils finally disappears. The drag coefficient decreases dramatically and a flow similar to the design condition is obtained. This plot illustrates the poor off-design performance of the original Busemann airfoil. During acceleration, the design condition ($c_d = 0.00341$) can not be obtained at Mach number 1.7 and the drag coefficient is much higher ($c_d = 0.08728$). Because of the flow-hysteresis effect, the Busemann airfoil has different c_d during acceleration and deceleration as shown in Figure 10.

Figure 13 shows the pressure coefficient of the original Busemann airfoil during deceleration. As before, the angle of attack is also set to zero and the resulting flow field is zero-lift. Although the Busemann airfoil shows decent performance in the range near design Mach number, high drag occurs when the Mach number further decreases during deceleration. Because a strong bow shock wave is formed before the airfoil when the Mach number changes from 1.61 to 1.6, the drag increases dramatically from 0.00603 to 0.08886, substantially higher than that of the standard diamond airfoil. The flow is choked at the maximum thickness section and a subsonic area is formed. This is also a good demonstration of the poor off-design performance of the Busemann airfoil since the drag of the Busemann airfoil will be greater than the standard diamond airfoil for $M_a \leq 1.6$.

In conclusion, compared to the standard diamond airfoil of the same thickness, the Busemann airfoil produces a higher drag in the low Mach number zone (below the designed Mach number). In addition, we need to accelerate the Busemann biplane to a higher Mach number, while producing higher drag and then decrease velocity to get the design condition. Thus, the Busemann biplane airfoil need to be redesigned so that the high drag zone caused by the flow-hysteresis and choke-flow phenomenon can be avoided or at least reduced.

The separated diamond design is the first biplane design calculated here to avoid the flow-hysteresis and choke-flow phenomenon. Figure 14 shows the comparison of drag coefficients of the standard diamond airfoil, the separated diamond airfoil and the Busemann airfoil. The Mach number ranges from 0.3 to 3.3 just as in Figure 10. From the plot, we can see that the c_d line of separated diamond airfoil agrees very well

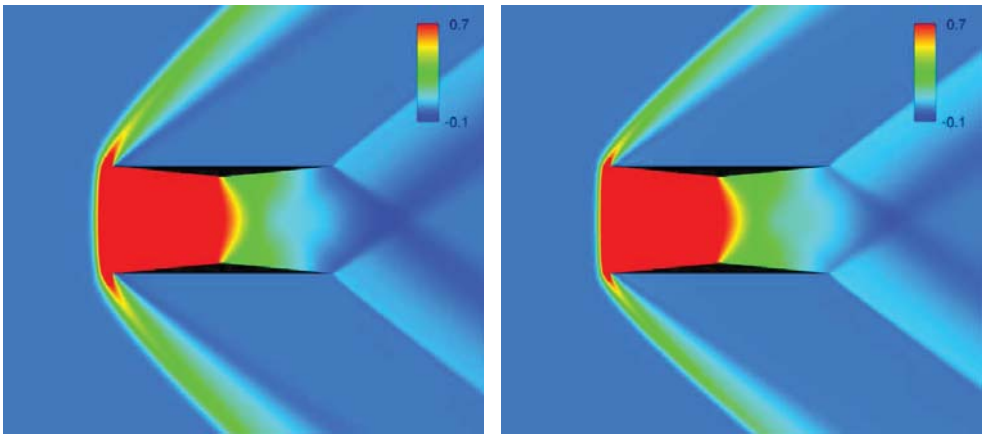

(a) M_∞=1.7,c_d=0.08728

(b) M_∞=1.8,c_d=0.08575

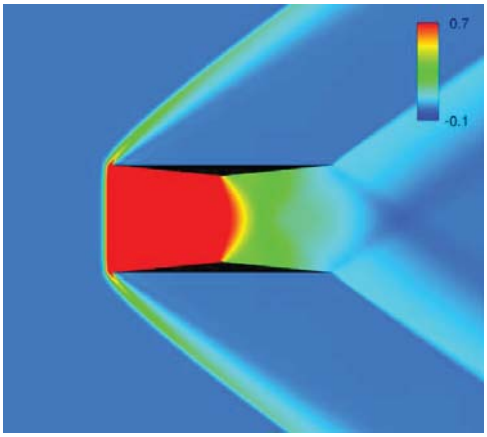

(c) M_∞=1.9,c_d=0.08415

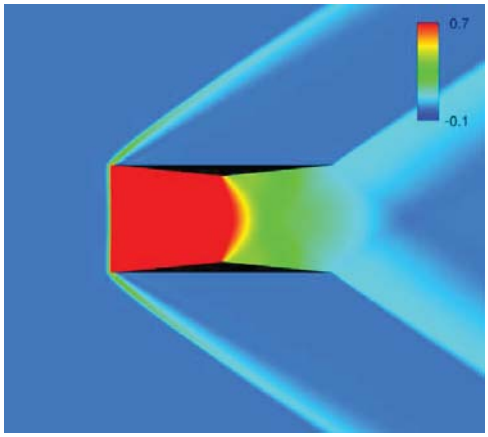

(d) M_∞=2.0,c_d=0.08223

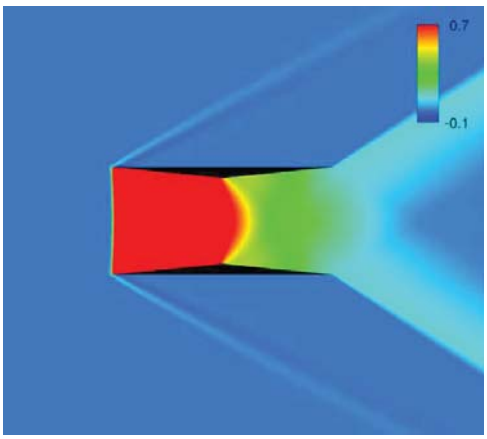

(e) M_∞=2.1,c_d=0.08009

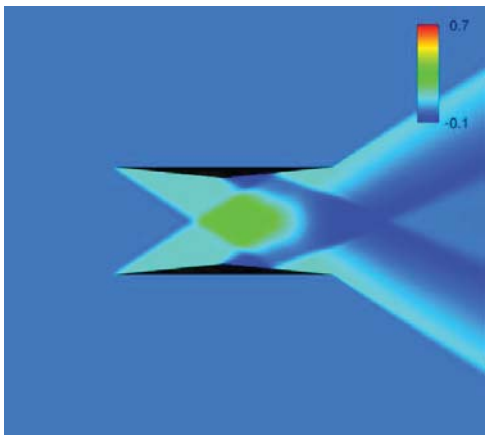

(f) M_∞=2.11,c_d=0.00950

Figure 12. **C_p-contours of the Busemann biplane with zero-lift during acceleration**

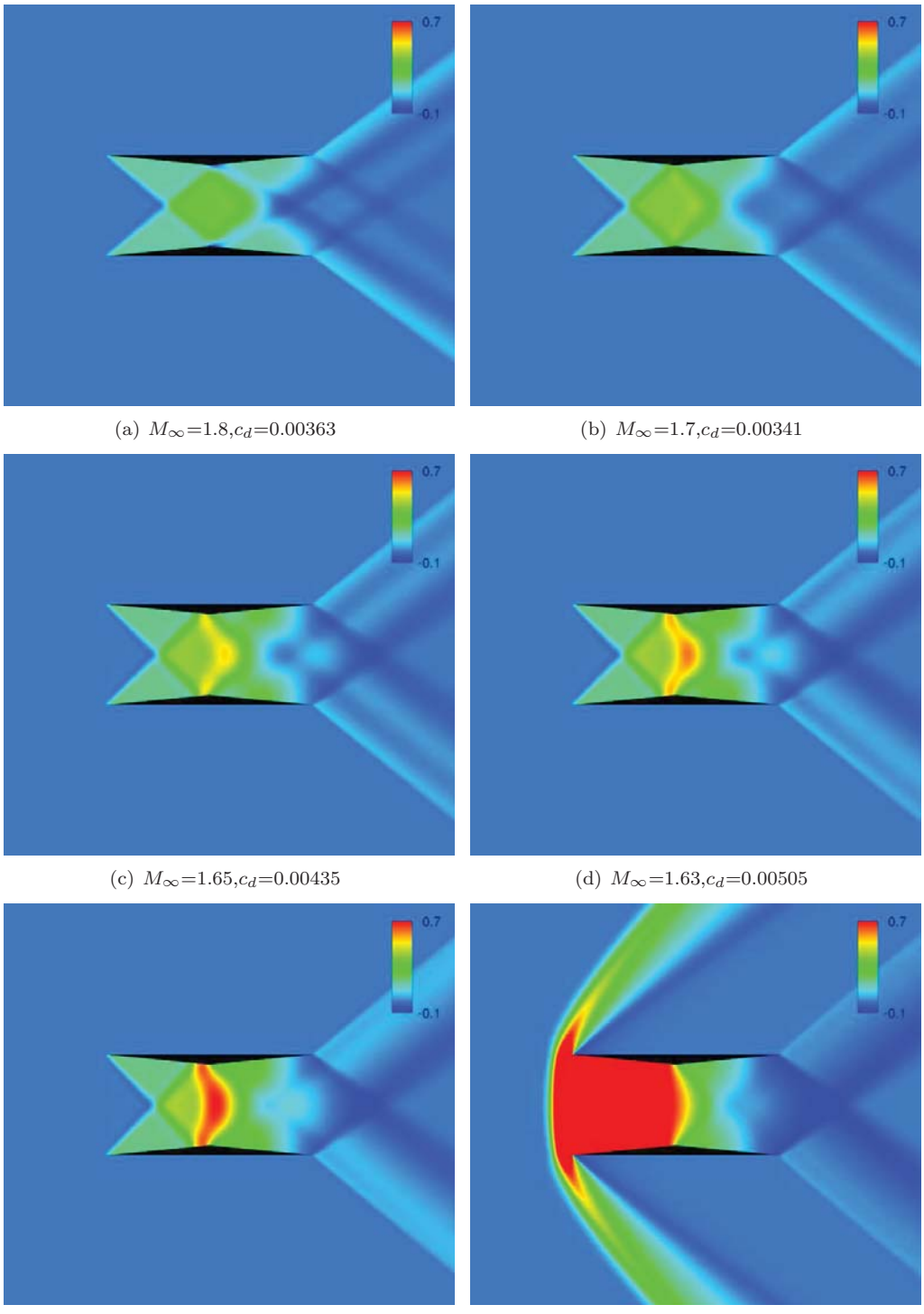

(a) M_∞=1.8,c_d=0.00363

(b) M_∞=1.7,c_d=0.00341

(c) M_∞=1.65,c_d=0.00435

(d) M_∞=1.63,c_d=0.00505

(e) M_∞=1.61,c_d=0.00603

(f) M_∞=1.6,c_d=0.08886

Figure 13. C_p**-contours of the Busemann biplane with zero-lift during deceleration**

with the standard diamond airfoil. In the separated diamond airfoil case, no choke-flow or flow hysteresis phenomenon happened. However, since the separated diamond airfoil shows the same drag characteristics as the standard diamond airfoil, which produces higher c_d at our design condition (Mach number 1.7) than the Busemann airfoil, we hope to optimize the Busemann airfoil by choosing a shape combining Busemann airfoil and the separated diamond airfoil designs.

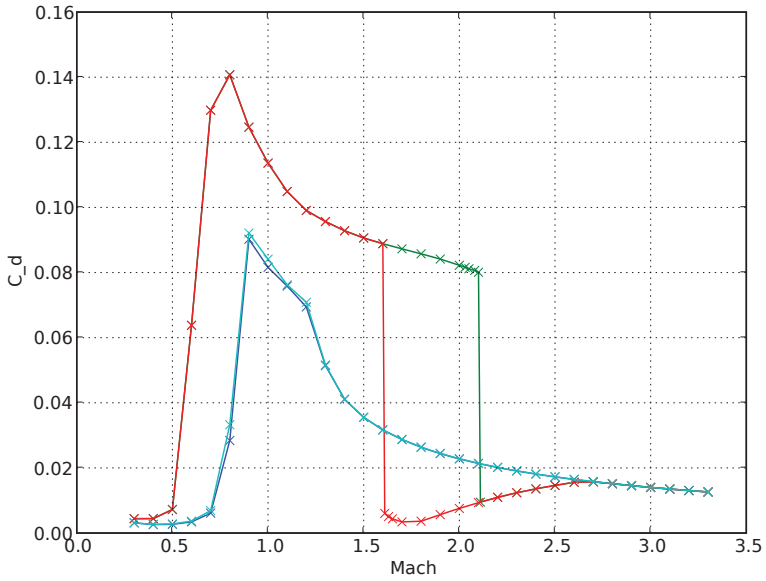

Figure 14. c_d **plot for different airfoils at zero-lift condition.**

B. Optimized design under Non-lifting Condition

The initial computational grid is shown in Figure 11. Multiple design points are used in the optimization process since the original Busemann airfoil showed flow hysteresis and choke-flow phenomenon during acceleration and deceleration. For this multi-point design case, the objective function used here is a weighted average of c_d, which can be written as:

$$I = \sum_{i=1}^{n} w_i I_i \tag{11}$$

Because the wave drag of a biplane airfoil will be much smaller when the flow is unchoked, we want the strong bow shock wave be swallowed before the design Mach number. The multiple design points and the corresponding weight used in this research are given in Table 3. Here equal weight is given to each design point. Actually, higher weight could be put on the most important design Mach number to produce lower drag at that point.

Mach	1.1	1.2	1.3	1.4	1.5	1.6	1.7	1.6	1.5	1.4	1.3	1.2	1.1
Weight	$\frac{1}{13}$	$\frac{1}{13}$	$\frac{1}{13}$	$\frac{1}{13}$	$\frac{1}{13}$	$\frac{1}{13}$	$\frac{1}{13}$	$\frac{1}{13}$	$\frac{1}{13}$	$\frac{1}{13}$	$\frac{1}{13}$	$\frac{1}{13}$	$\frac{1}{13}$

Table 3. Multiple design points and the corresponding weight

The lift coefficient c_l is fixed to zero and a constant thickness constraint is used during the optimization

process. In addition, the points of the maximum thickness section of the Busemann airfoil are fixed so that the optimized airfoil has the same throat area as the original Busemann airfoil.

Figure 15 shows a comparison of the optimized biplane airfoil with the original Busemann airfoil. We can see that the optimized biplane airfoil has the same thickness as the original Busemann airfoil at all corresponding positions and the thickest position is fixed by the constraints. The wedge angles of these two airfoils are the same. The leading edges and trailing edges of the optimized biplane airfoil bend towards the center. The two components of the optimized biplane airfoil are still symmetric with respect to the Y-axis in Figure 15 due to the zero-lift condition.

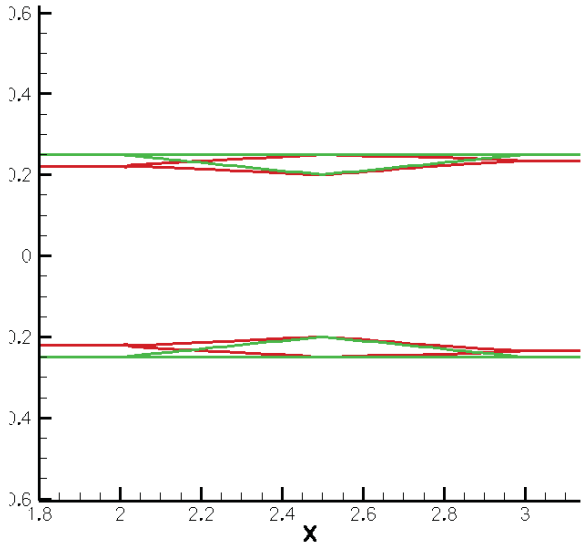

Figure 15. Comparison of the baseline Busemann airfoil and the optimized biplane airfoil. The red line indicates the baseline Busemann airfoil; the blue line indicates the optimized biplane airfoil.

The drag coefficients for each design point are compared in Table 4. From the table, we can see the baseline Busemann airfoil is choked at all Mach numbers in the optimization range, while the optimized biplane is unchoked at a wider range (from 1.6 to 1.7 to 1.4). And even at the choked condition, the optimized biplane airfoil has much lower drag than the baseline Busemann airfoil.

Mach	1.1	1.2	1.3	1.4	1.5	1.6	1.7	1.6	1.5	1.4	1.3	1.2	1.1
Baseline	1050	996	957	928	906	889	873	889	906	928	957	996	1050
Optimized	527	473	419	376	332	112	106	112	127	152	419	473	527

Table 4. c_d comparison at zero lift condition (1 count = 0.0001)

Figure 16 shows the comparison of the drag coefficient for the optimized biplane airfoil with the standard diamond airfoil and the baseline Busemann airfoil. From the plot, we can see there are still two separated c_d lines for the optimized biplane airfoil, which means that the flow hysteresis and choked-flow effect still exist. However, the flow hysteresis area has been greatly reduced. We also found from the plot that the drag increase due to the choked-flow also becomes much smaller than that of the original Busemann airfoil. From the plot, we can see that the drag of the optimized biplane airfoil is also smaller than that of the original Busemann airfoil in the subsonic area (Mach number 0.5 to 0.9) although it is higher than the standard diamond airfoil below Mach number 0.8. Considering both subsonic and supersonic conditions, we see the optimized biplane airfoil greatly reduces the wave drag. At the design condition (Mach number 1.7), the wave drag of the optimized biplane airfoil is higher ($c_d = 0.01064$) than that of original Busemann airfoil (c_d

= 0.00341). This is because we focused on reducing the choked-flow and flow hysteresis effect in this design and optimized the airfoil for multiple Mach numbers with equal weight. To alleviate this problem, we could put more weight on the design Mach number 1.7 during the optimization process.

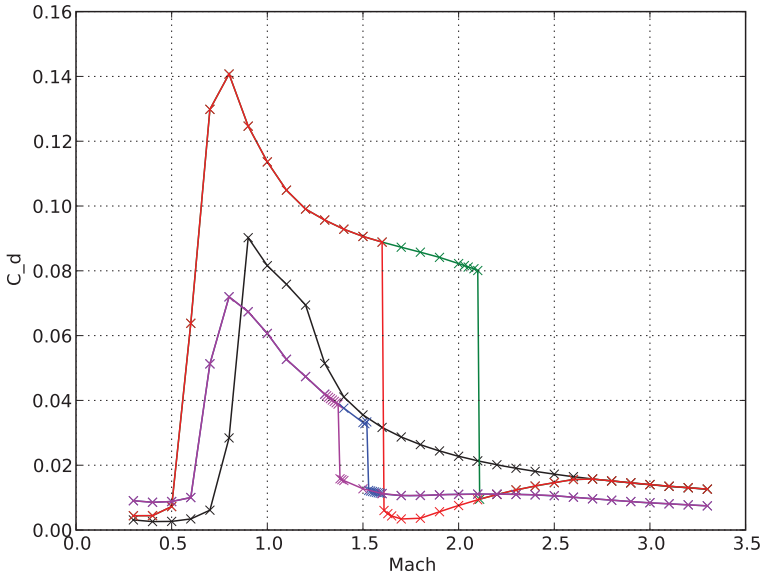

Figure 16. c_d **plot for different airfoils at zero-lift conditions.**

We now examine the details of the accelerating and decelerating conditions. Figure 17 and Figure 18 show the pressure coefficient distribution of the optimized biplane airfoil during acceleration and deceleration respectively. During acceleration (Figure 17), the flow hysteresis effect still forms a bow shock wave in front of the airfoil. When the Mach number increases from 1.52 to 1.53 (compared with Busemann at Mach number 2.11), the shock wave is swallowed into the two airfoils and the wave drag decreased greatly from 0.03336 to 0.01221. During deceleration (Figure 18), we can also observe that there is also a choked-flow phenomenon. But the optimized biplane airfoil shifts the choked flow at the maximum thickness sections to a lower Mach number (Mach number 1.37 here) than the original Busemann airfoil (Mach number 1.6).

C. Busemann Biplane under Lifting Condition

In the real word, we care more about the lifting condition than the zero-lift condition. Here, we apply our optimization method to the lifting condition. Two lifting cases are tested - c_l 0.05 and 0.1. The same number of mesh points and grid configurations are used in all the computations. Figure 19 shows the comparison of the drag coefficient of the standard diamond airfoil and the original Busemann airfoil over a range of Mach numbers (0.3 to 3.3) for these two lift coefficients. From the plot, we can see the c_d plot for the Busemann airfoil still splits into two lines, one for acceleration and the other for deceleration in both cases. This split implies flow hysteresis and choke-flow phenomenon. At Mach number 1.7, the Busemann airfoil produces much less wave drag than the standard diamond airfoil does because of the favorable shock-shock interaction effect.

At both lifting conditions, the bow shock wave in front of the airfoil results in substantially higher drag at high Mach numbers (about 2.08) during acceleration. When the Mach number increases, the bow shock wave is swallowed and the subsonic region between the two airfoils finally disappears. The flow-hysteresis phenomenon still exists as it does at the zero-lift condition. During deceleration,the wave drag is small (an

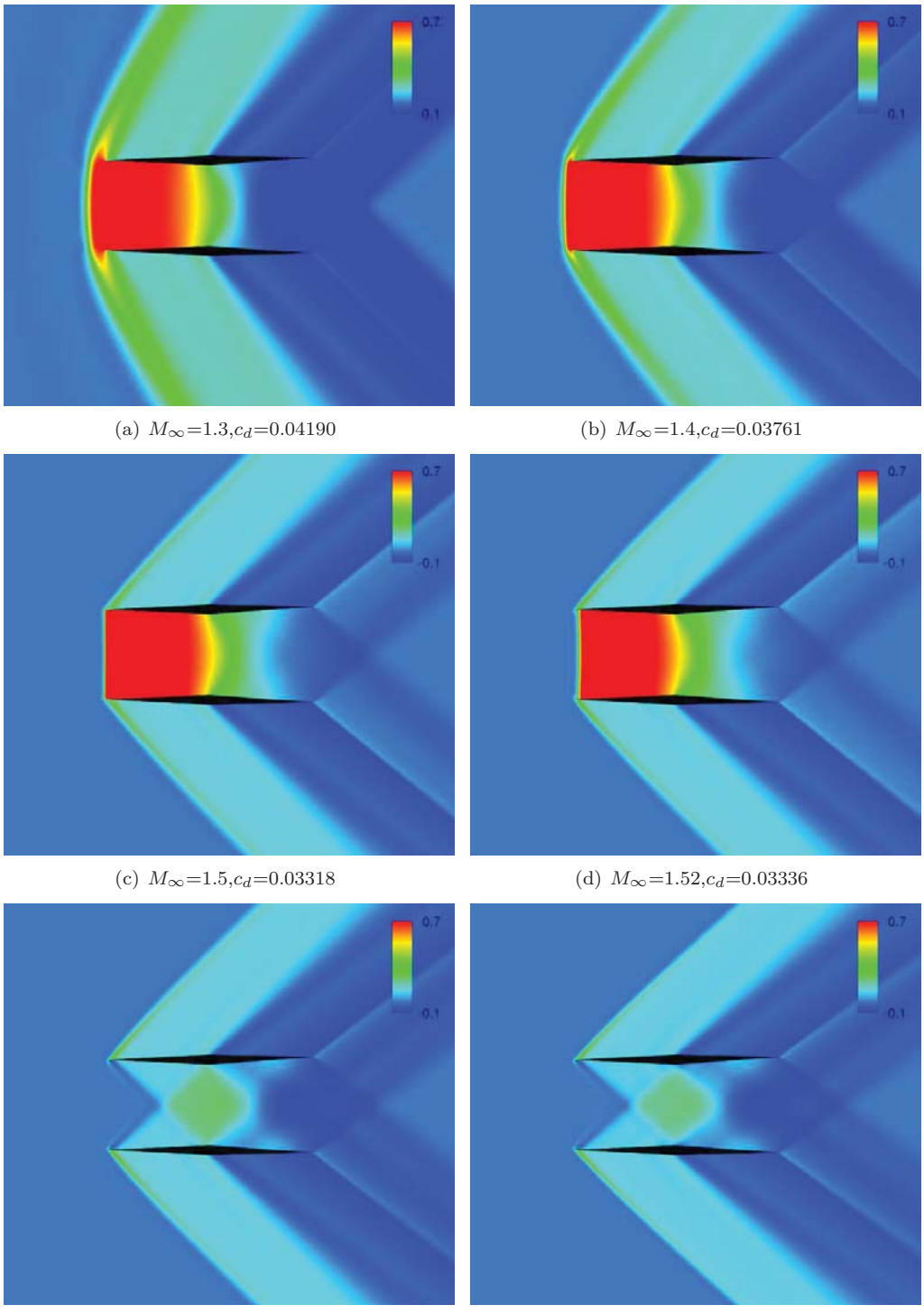

(a) M_∞=1.3,c_d=0.04190

(b) M_∞=1.4,c_d=0.03761

(c) M_∞=1.5,c_d=0.03318

(d) M_∞=1.52,c_d=0.03336

(e) M_∞=1.53,c_d=0.01221

(f) M_∞=1.6,c_d=0.01125

Figure 17. C_p**-contours of the optimized biplane with zero-lift during acceleration**

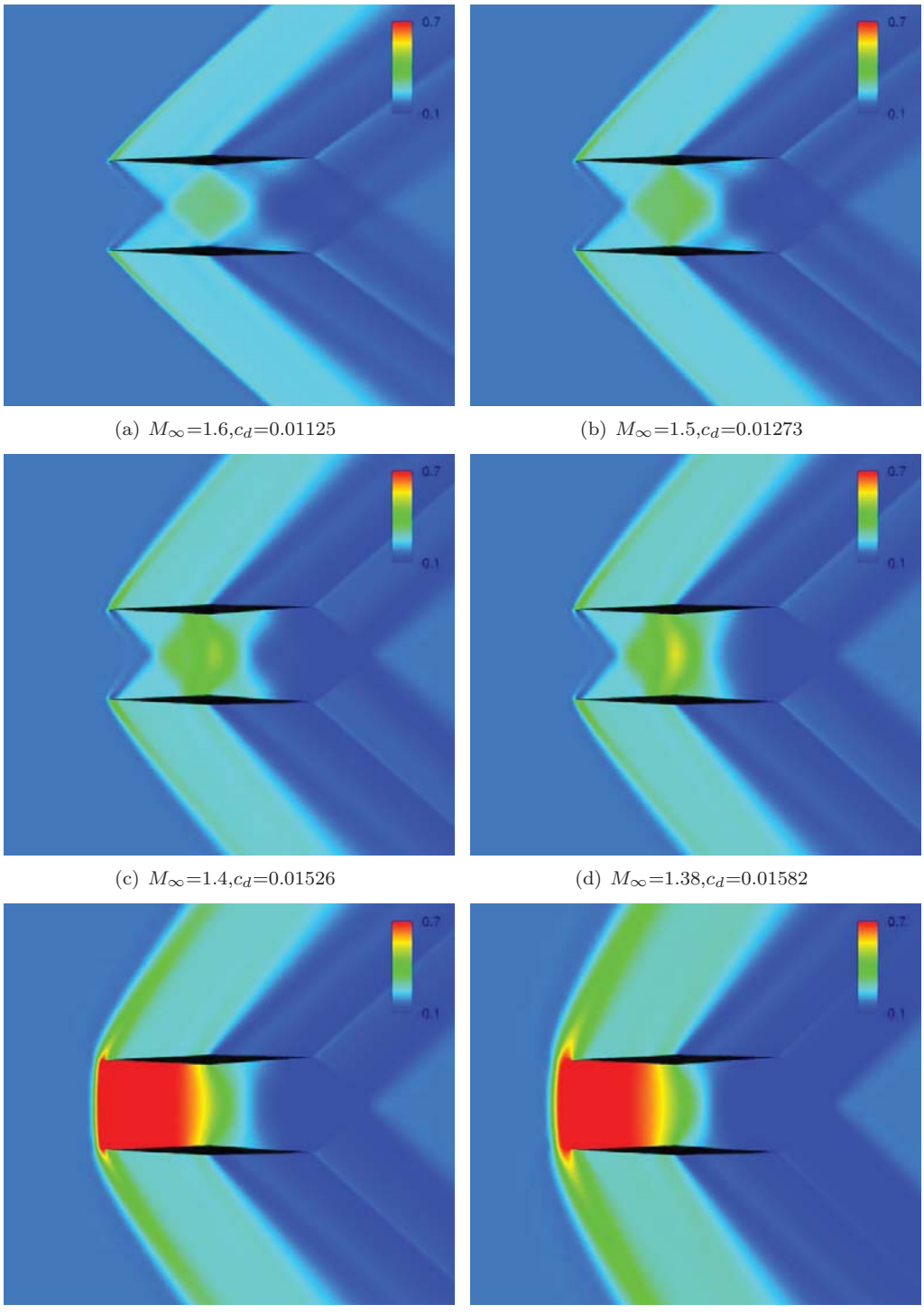

(a) M_∞=1.6,c_d=0.01125

(b) M_∞=1.5,c_d=0.01273

(c) M_∞=1.4,c_d=0.01526

(d) M_∞=1.38,c_d=0.01582

(e) M_∞=1.37,c_d=0.03886

(f) M_∞=1.3,c_d=0.04191

Figure 18. C_p**-contours of the optimized biplane with zero-lift during deceleration**

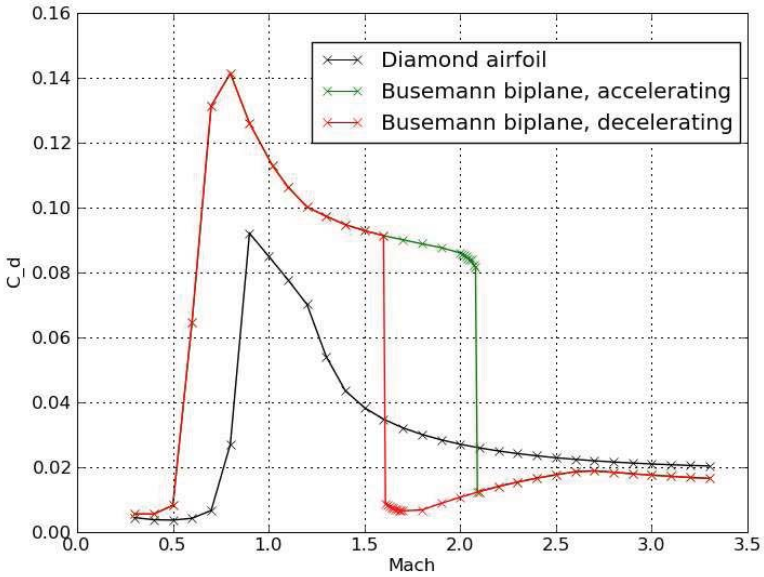

(a) $c_l = 0.05$

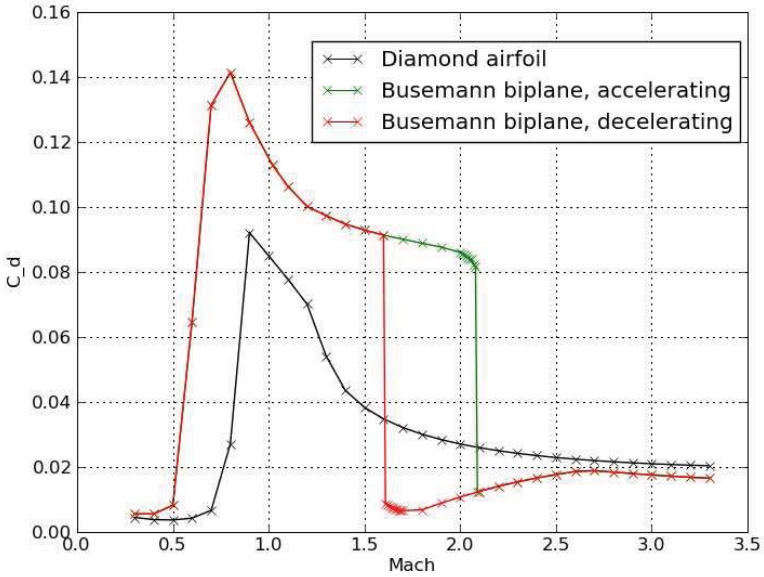

(b) $c_l = 0.1$

Figure 19. c_d plot of different airfoil at lifting condition

order of magnitude) until a strong bow shock wave forms in front of the airfoil when the Mach number decreases due to the choked-flow effect.

In conclusion, similar to the zero-lift condition, the Busemann airfoil produces substantially lower wave drag than the standard diamond airfoil of the same thickness at Mach number 1.7 due to the favorable shock-shock interaction effect when c_l is fixed. However, the Busemann airfoil demonstrates poor off-design performance during acceleration and deceleration caused by the flow-hysteresis and choke-flow effect.

1. Optimized designs at lifting conditions

Just as at the zero-lift condition, multiple design points are used to optimize the biplane airfoil during acceleration and deceleration. A fixed thickness constraint is applied. The points at the maximum thickness section are fixed. The cost function is still the weighted c_d at all design points.

The comparison of the drag coefficient for both cases are given in Table 5 and Table 6.

Mach	1.1	1.2	1.3	1.4	1.5	1.6	1.7	1.6	1.5	1.4	1.3	1.2	1.1
Baseline	1054	1000	962	934	913	896	881	896	913	934	962	1000	1054
Optimized	520	472	425	388	351	119	112	119	134	158	425	472	520

Table 5. c_d comparison for $c_l = 0.05$ (1 count = 0.0001)

Mach	1.1	1.2	1.3	1.4	1.5	1.6	1.7	1.6	1.5	1.4	1.3	1.2	1.1
Baseline	1066	1013	977	952	933	918	905	918	933	952	977	1013	1066
Optimized	535	489	446	413	377	136	131	136	149	173	446	489	535

Table 6. c_d comparison for $c_l = 0.1$ (1 count = 0.0001)

Figure 20 shows a comparison of the optimized biplane airfoil with the original Busemann airfoil for both lift coefficients. As can be seen, the optimized biplane airfoil still has the same thickness as the original Busemann airfoil at all corresponding positions and the maximum thickness position is fixed by the constraints. Both the leading edges and trailing edges of the optimized biplane airfoils bend towards the center. However, due to the lifting condition, the two components of the optimized airfoil are not symmetric.

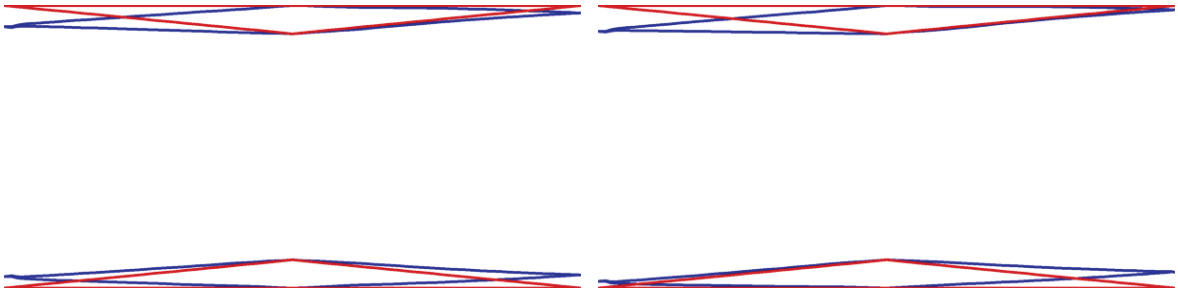

(a) $c_l = 0.05$ (b) $c_l = 0.1$

Figure 20. Comparison of baseline Busemann airfoil and the optimized biplane airfoil.

Figure 21 shows the comparison of the drag coefficient for the optimized biplane airfoil with the standard diamond airfoil and the original Busemann airfoil at $c_l = 0.05$ and $c_l = 0.1$. Just as at the zero-lift condition, flow-hysteresis and choke-flow phenomenon still exist for the optimized Busemann airfoil. During acceleration, the wave drag of the optimized biplane airfoil is smaller than the wave drag of the original

Busemann airfoil during the whole Mach number range (from 0.3 to 3.3). For deceleration, the wave drag of the optimized biplane airfoil is smaller than the wave drag of the original Busemann airfoil except for the Mach number range 1.6 to 2.1. Therefore, it is possible to greatly reduce the wave drag of the Busemann airfoil by using our multiple design point method.

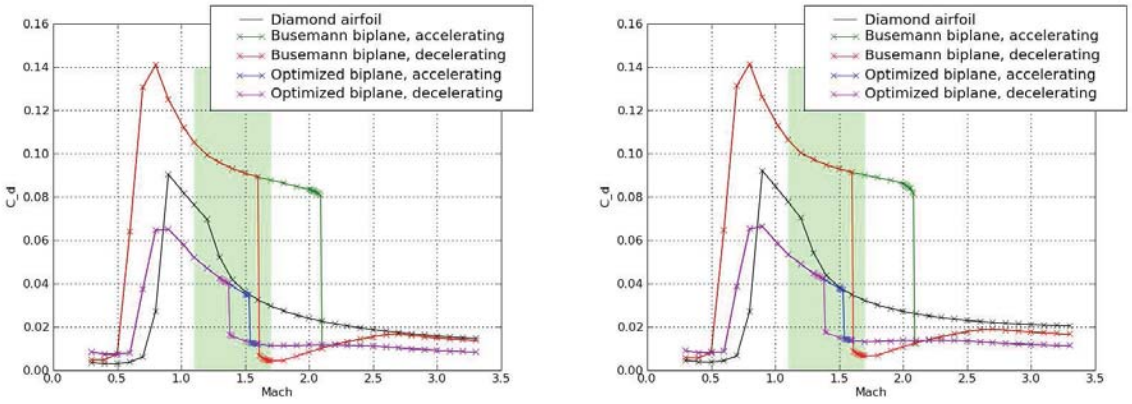

(a) $c_l = 0.05$ (b) $c_l = 0.1$

Figure 21. c_d plot of different airfoils at lifting condition.

The pressure coefficient distribution of the optimized biplane airfoil during acceleration and deceleration at $c_l = 0.05$ and $c_l = 0.1$ show the flow-hysteresis and choke-flow phenomenon are similar to the original Busemann airfoil. However, during acceleration, the bow shock wave is swallowed at a lower Mach number (Mach number 1.54). During deceleration, the optimized biplane airfoil shifts the choked flow at the maximum thickness section to a lower Mach number (Mach number 1.38).

D. Sensitivity Tests

To check whether the optimized biplane airfoil is robust at other off-design conditions, two sensitivity studies have been performed. The optimized biplane airfoil for zero lift is used in these studies.

Figure 22(a) shows the sensitivity to the angle of attack. In our simulation, the angle of attack is a uniform random number between 0 and 1 degree. Twenty-five different angle of attack conditions are tested. From the plot, we can see that the drag coefficient of the optimized biplane airfoil only change very small at all different angle of attack conditions. The flow hysteresis range (wave drag coefficient line splitting rang) for all cases are within 0.01 Mach number variation. Thus the optimized design is not very sensitive to the variation of the angle of attack.

Figure 22(b) shows the sensitivity to the separation distance (the distance between two airfoils). The separation distance is a uniform random number between $\pm(0.02)$ chord length and again 25 different cases are tested. The separation distance of biplane airfoil is an important parameter because the shock wave from the leading edge will arrive different part of the opposite airfoil such that the pressure over the airfoil surface will change obviously. Thus we can see the wave drag in the Mach number range $(1.6, 2.5)$ for different cases are about 20% variation. For different separation distance cases, the flow will be unchoked at different Mach number. Thus the flow hysteresis ranges are not the same as the angle of attack sensitivity test. When the Mach number is higher than 2.6, the shock wave from the leading edge will not interact with the opposite airfoil component. The wave drag for all different separation distance case will be the same.

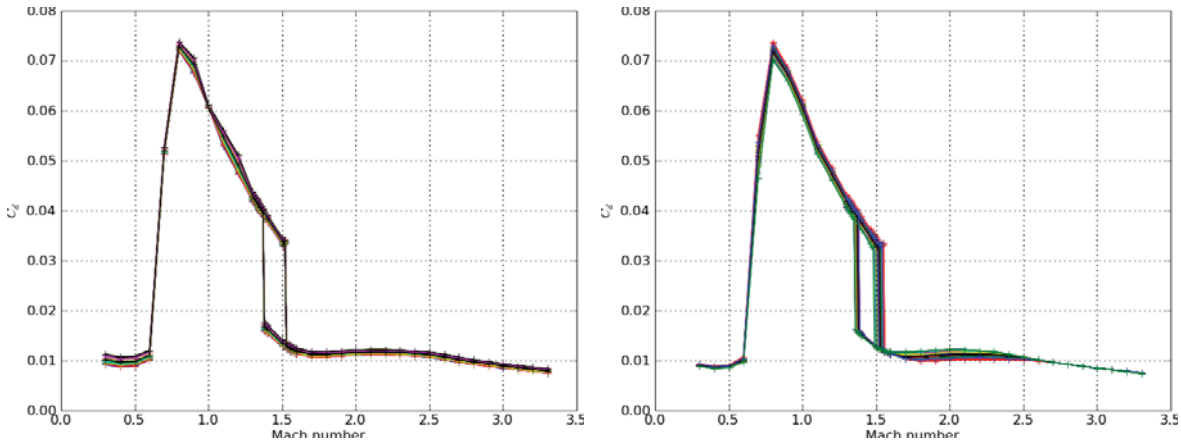

(a) To angle of attack

(b) To separation distance

Figure 22. Sensitivity tests.

VI. Conclusions

In this paper, the favorable shock wave interaction of the supersonic biplane airfoil is studied. Two-dimensional numerical simulation results show that the Busemann biplane airfoil produces very low wave drag at design condition due to the perfect shock-expansion wave cancellation. But for off-design conditions, the Busemann biplane airfoil performance is poor. To overcome the choked-flow and flow-hysteresis problems of the Busemann biplane at off-design conditions, the inviscid compressible flow (Euler) optimization techniques based on control theory have been applied.

In order to obtain an optimized supersonic airfoil with lower wave drag within the given optimization Mach number range, a multiple design point strategy is employed. The optimized biplane airfoil shows good performance at both design and off-design conditions. The flow-hysteresis phenomenon of the optimized airfoil still exists but the area is greatly reduced compared to that of the baseline Busemann biplane and the wave drag caused by choked flow is also much lower. For inviscid flow, the wave drag of the optimized biplane airfoil is lower than that of the diamond airfoil with the same total thickness throughout the optimization range. The two sensitivity studies show that the optimized design is robust and not very sensitive to the change of the angle of attack or the separation distance.

References

[1]Busemann, A., *Aerodynamic Lift at Supersonic Speeds*, No. 6, Luftfahrtforschung, 12th ed., Oct 1935, pp. 210–220.

[2]Moeckel, W. E., "Theoretical aerodynamic coefficients of the two-dimensional supersonic biplane," Tech. Rep. 1316, NACA, 1947.

[3]Licher, R., "Optimum Two-Dimensional Multiplanes in Supersonic Flow," Tech. Rep. SM-18688, Douglass Aircraft Co., 1955.

[4]Tan, H. S., "The aerodynamics of supersonic biplanes of finite span," Tech. Rep. 52-276, WADC, 1950.

[5]Ferri, A., *Elements of aerodynamics of supersonic flow*, The Macmillan Company, New York, 1949, Also published from Dover Phoenix Edition,Dover Publications, Inc., New York, 2005.

[6]Igra, D. and Arad, E., "A parametric study of the Busemann biplane phenomena," *Shock Waves*, Vol. 16, No. 33, February 2007, pp. 269–273.

[7]Kusunose, K., Matsushima, K., Goto, Y., Yamashita, H., Yonezawa, M., Maruyama, D., and Nakano, T., "A Fundamental Study for the Development of Boomless Supersonic Transport Aircraft," *44rd AIAA Aerospace Sciences Meeting and Exhibit*, AIAA 2006-654, January 2006.

[8]Maruyama, D., Matsushima, K., Kusunose, K., and Nakahashi, K., "Aerodynamic Design of Biplane Airfoils for Low Wave Drag Supersonic Flight," *24th Applied Aerodynamics Conference*, AIAA 2006–3323, San Francisco, California, June 2006.

[9]Maruyama, D., Matsuzawa, T., Kusunose, K., Matsushima, K., and Nakahashi, K., "Consideration at Off-design Con-

ditions of Supersonic Flows around Biplane Airfoils," *45th AIAA Aerospace Sciences Meeting and Exhibit*, AIAA 2007-687, January 2007.

[10]Kusunose, K., Yonezawa, M., Obayashi, S., and Kusunose, K., "A Study of Busemann-type Biplane for Avoiding Choked Flow," *45th AIAA Aerospace Sciences Meeting and Exhibit*, AIAA 2007-688, Reno, Nevada, January 2007.

[11]Kuratani, N., Ogawa, T., Yamashita, H., Yonezawa, M., and Obayashi, S., "Experimental and Computational Fluid Dynamics around Supersonic Biplane for Sonic-Boom Reduction," *13th AIAA/CEAS Aeroacoustics Conference (28th AIAA Aeroacoustics Conference)*, AIAA 2007-3674, 2007.

[12]Kashitani, M., Yamaguchi, Y., Kai, Y., and Hirata, K., "Preliminary Study on Lift Coefficient of Biplane Airfoil in Smoke Wind Tunnel," *46th AIAA Aerospace Sciences Meeting and Exhibit*, AIAA 2008-349, January 2008.

[13]Liepmann, H. and Roshko, A., *Elements of Gasdynamics*, chap. Waves in Supersonic Flow, Dover Publications, Inc., Mineola, New York, 1957, pp. 107–118.

[14]Goto, Y., Kusunose, K., Yamashita, H., and Yonezawao, M., "Numerical Analysis of Busemann's Biplane for Application to Boomless Supersonic Transport," *JSME 17th Computational Mechanics Conference*, Sendai, Japan, November 2004, pp. 117–118.

[15]Kusunnose, K., "A Wake Integration Method for Airplane Drag Prediction," *The 21st Century COE Program International COE of Flow Dynamics Lecture Series*, Vol. 3, pp. 65–70.

[16]Jameson, A., Schmidt, W., and Turkel, E., "Numerical solutions of the Euler equations by finite volume methods with Runge-Kutta time stepping schemes," AIAA paper 81-1259, January 1981.

[17]Jameson, A., "Steady State Solution of the Euler Equations for Transonic Flow," *In Proceedings of Symposium on Transonic, Shock and Multidimensional Flows*, edited by R. Meyer, Academic Press, Madison, WI, 1982, pp. 30–37.

[18]Jameson, A., "Multigrid algorithms for compressible flow calculations," *Proceedings of the 2nd European Conference on Multigrid Methods*, Princeton University Report MAE 1743, Cologne, October 1985.

[19]Jameson, A., Baker, T., and Weatherill, N., "Calculation of Inviscid Transonic Flow Over a complete Aircraft," *AIAA 24th Aerospace Sciences Meeting*, AIAA paper 86–0103, Reno, January 1986.

[20]Jameson, A., "Solution of the Euler equations for two dimensional transonic flow by a multigrid method," *Applied Mathematics and Computations*, Vol. 13, 1983, pp. 327–356.